Published in final edited form as:
Cell Metab. 2013 February 5; 17(2): 210–224. doi:10.1016/j.cmet.2013.01.004.

MicroRNA-133 Controls Brown Adipose Determination in Skeletal Muscle Satellite Cells by Targeting Prdm16

Hang Yin[1], **Alessandra Pasut**[1], **Vahab D. Soleimani**[1], **C. Florian Bentzinger**[1], **Ghadi Antoun**[2], **Stephanie Thorn**[3], **Patrick Seale**[4], **Pasan Fernando**[3,5], **Wilfred van IJcken**[6], **Frank Grosveld**[6], **Robert A. Dekemp**[3], **Robert Boushel**[7], **Mary-Ellen Harper**[2], and **Michael A. Rudnicki**[1,*]

[1]Regenerative Medicine Program, Ottawa Hospital Research Institute, Ottawa, ON K1H 8L6, Canada [2]Department of Biochemistry, Microbiology, and Immunology, Faculty of Medicine, University of Ottawa, Ottawa, ON K1H 8M5, Canada [3]University of Ottawa Heart Institute, Ottawa, ON K1Y 4W7, Canada [4]Institute for Diabetes, Obesity, and Metabolism, University of Pennsylvania School of Medicine, Philadelphia, PA 19104, USA [5]Nordion, Ottawa, ON K2K 1X8, Canada [6]Department of Cell Biology and Genetics, Erasmus MC, Dr. Molewaterplein 50, 3015 GE Rotterdam, The Netherlands [7]Department of Biomedical Sciences, University of Copenhagen, Department of Anaesthesia, Bispebjerg Hospital, 2400 Copenhagen NV, Denmark

SUMMARY

Brown adipose tissue (BAT) is an energy-dispensing thermogenic tissue that plays an important role in balancing energy metabolism. Lineage-tracing experiments indicate that brown adipocytes are derived from myogenic progenitors during embryonic development. However, adult skeletal muscle stem cells (satellite cells) have long been considered uniformly determined toward the myogenic lineage. Here, we report that adult satellite cells give rise to brown adipocytes and that microRNA-133 regulates the choice between myogenic and brown adipose determination by targeting the 3′UTR of *Prdm16*. Antagonism of microRNA-133 during muscle regeneration increases uncoupled respiration, glucose uptake, and thermogenesis in local treated muscle and augments whole-body energy expenditure, improves glucose tolerance, and impedes the development of diet-induced obesity. Finally, we demonstrate that miR-133 levels are downregulated in mice exposed to cold, resulting in de novo generation of satellite cell-derived brown adipocytes. Therefore, microRNA-133 represents an important therapeutic target for the treatment of obesity.

INTRODUCTION

Obesity is associated with increased risks of type 2 diabetes, cardiovascular diseases, and cancer and thus poses a demanding challenge for global health care. Although diet and exercise are well-known defenses against obesity, the exacerbating epidemic of obesity has raised a major interest to develop alternative therapeutic strategies. Two distinct types of adipose tissues exist—white and brown. When dietary energy exceeds total body energy needs, the energy is stored mainly as triglycerides in white adipocytes. By contrast, brown

*Correspondence: mrudnicki@ohri.ca, http://dx.doi.org/10.1016/j.cmet.2013.01.004.

SUPPLEMENTAL INFORMATION

Supplemental Information includes six figures, three tables, Supplemental Experiemental Procedures, and Supplemental References and can be found with this article at http://dx.doi.org/10.1016/j.cmet.2013.01.004.

adipocytes are specialized to dissipate energy in the form of body heat (thermogenesis) and are characterized by expression of uncoupling protein Ucp1 in their abundant mitochondria (Frontini and Cinti, 2010).

Active brown adipose tissue (BAT) can provide a natural defense against obesity. However, BAT is relatively scarce in adult humans, and its prevalence was not unequivocally recognized until recently (Cypess et al., 2009; Nedergaard et al., 2007; Ouellet et al., 2012; Saito et al., 2009; van Marken Lichtenbelt et al., 2009; Virtanen et al., 2009; Zingaretti et al., 2009). Intriguingly, the level of BAT activity in adult humans is negatively correlated to body mass index (Cypess et al., 2009; Nedergaard et al., 2010; Pfannenberg et al., 2010; van Marken Lichtenbelt et al., 2009). Experimental induction of BAT function in animal models is associated with a lean and healthy phenotype (Ghorbani and Himms-Hagen, 1997; Kopecky et al., 1995). As such, expanding and activating BAT thermogenesis opens a new avenue toward preventing/treating obesity and obesity-related metabolic disorders (Cypess and Kahn, 2010).

Lineage-tracing experiments have indicated that BAT is derived during embryogenesis from Pax7/Myf5-expressing skeletal muscle precursors located within dermomyotome (Atit et al., 2006; Lepper and Fan, 2010; Seale et al., 2008). Importantly, Prdm16, a zinc-finger transcription factor, has been demonstrated to be necessary and sufficient to establish the identity of the BAT lineage (Seale et al., 2007, 2008). In vitro, loss of function of Prdm16 promotes the myogenic differentiation of committed preadipocytes isolated from BAT, whereas Prdm16 gain of function leads to brown adipogenesis of the C2C12 myoblast cell line and myoblasts isolated from newborn mice (Seale et al., 2008). Similarly, Prdm16 is also both necessary and sufficient for the emergence of beige adipocytes in subcutaneous WAT (browning), which is linked with improved metabolic phenotypes (Seale et al., 2011).

Prdm16 determines BAT identity by activating the complete complement of brown fat genes while also repressing WAT-specific (Kajimura et al., 2008) and muscle-specific programs (Seale et al., 2008). Notably, ablation of Prdm16 in BAT abolishes the expression of brown adipocyte-specific thermogenic genes (e.g., *Ucp1*), yet spares the terminal adipogenic differentiation and the expression of adipogenic markers that are common to both white and brown adipocytes (Seale et al., 2008). As such, Prdm16 represents a “master regulator” of brown adipogenesis particularly critical for brown adipose lineage determination.

The potent fate-switching function of Prdm16 in vitro implies that its expression be tightly regulated in myogenic cells in vivo. Satellite cells are adult skeletal muscle stem cells, which reside closely juxtaposed with contractile myofibers beneath the basal lamina (Chargé and Rudnicki, 2004). Satellite cells are quiescent in vivo under physiological conditions, whereas they can be activated in response to resistance training or muscle injury. When activated, satellite cells migrate from the myofibers and proliferate as committed myogenic precursors (myoblasts), which in turn undergo terminal myogenic differentiation (myogenesis) and fuse into multinucleated muscle cells (myotubes) (Chargé and Rudnicki, 2004). Notably, satellite cells are believed to be uniformly committed to the myogenic lineage, and it has been reported that they do not differentiate into adipocytes in vitro (Joe et al., 2010). This is consistent with the observation that Prdm16 is not detectable in satellite cells nor their daughter myogenic precursor cells (Seale et al., 2011).

Here we show that satellite cells are multipotent and can give rise to both myogenic and brown adipogenic lineages. The brown adipose determination of satellite cells is controlled by a myogenic microRNA, miR-133 that directly targets the 3′UTR of the *Prdm16* mRNA to repress Prdm16 expression. Inhibition of microRNA-133 during muscle regeneration elicits brown adipogenic commitment of satellite cells in vivo and induces their

differentiation into interstitial brown adipocytes. Cold exposure results in downregulation of miR-133 and de novo generation of satellite cell-derived brown adipocytes. Taken together, our data reveal a central function of miR-133 in controlling Prdm16-dependent lineage determination of satellite cells and suggest a promising strategy for inducing active BAT in vivo from skeletal muscle stem cells.

RESULTS

Single Satellite Cells Are Multipotent and Differentiate into Brown Adipocytes

In adult muscle, satellite cells are characterized by their specific expression of Pax7 in both quiescent and activated states (Seale et al., 2000). To investigate the capability of satellite cells in adult skeletal muscle to undergo brown adipogenic differentiation, we utilized a Cre/LoxP-based system for satellite cell lineage tracing (Nishijo et al., 2009). *Pax7-CreER;R26R-tdTomato* mice were injected with tamoxifin for 5 consecutive days at 6 weeks of age to induce permanent tdTomato expression in satellite cells and their descendants (see Figure S1A online).

From the extensor digitorum longus (EDL) muscles of these mice, we isolated single myofibers (n > 600), carrying labeled satellite cells embedded within their native niche, and cultured them under established proadipogenic conditions (Seale et al., 2008). We observed adipocytes at a low frequency, characterized by the presence of oil droplets and expression of cytoplasmic Perilipin A (a marker for differentiated adipocytes), mixed together with elongated multinucleated myotubes (Figure 1A). Importantly, these adipocytes were brown adipocytes, as evidenced by their nuclear expression of Prdm16 (Figure 1A). As expected, all multinucleated myotubes were labeled with tdTomato, indicating their satellite cell origin. Notably, Prdm16^{pos} brown adipocytes were similarly labeled with tdTomato, indicating that they derived from Pax7-expressing satellite cells (Figure 1A). Overall, satellite-cell-derived brown adipocytes (SC_BA) accounted for 0.1% of tdTomato-labeled cells in these cultures. By contrast, brown adipogenic differentiation of satellite cells was not observed under promyogenic culture conditions (Kuang et al., 2007) (Figure S1B).

Satellite cells represent a heterogeneous population containing stem cells and committed cells (Wang and Rudnicki, 2012). By lineage tracing, we have previously identified a satellite stem cell population (Pax7^{pos}, Myf5-Cre-YFP^{neg}) that can undergo asymmetric cell divisions to generate committed satellite myogenic progenitors (Pax7^{pos}, Myf5-Cre-YFP^{pos}) (Kuang et al., 2007). To measure the potential of these two satellite cell subpopulations to undergo brown adipogenesis, we employed fluorescence-activated cell sorting (FACS) to isolate total satellite cells from *Pax7-ZsGreen;Myf5-Cre;R26R-tdTomato* mice on the basis of their ZsGreen fluorescence (Bosnakovski et al., 2008), and further separate into satellite stem cell (ZsGreen^{pos}, Myf5-Cre-tdTomato^{neg}) and satellite myogenic progenitor (ZsGreen^{pos}, Myf5-Cre-tdTomato^{pos}) subpopulations by tdTomato fluorescence (Figures S1C and S1D).

To address whether these two subpopulations of satellite cells are multipotent (myogenic and adipogenic) at the clonal level, we sorted single satellite stem cells or satellite myogenic progenitors into individual wells (n > 2,000 for each cell type). The reliability of sorting single satellite cells into individual wells was confirmed by visual inspection of all wells (Figure S1E). We found that 6.5% of single satellite stem cell-derived clones contained exclusively oil red O (ORO)-positive adipocytes, whereas this kind of clone was not observed from satellite myogenic progenitor clones (Figure 1B, left). Notably, 1.6% of satellite stem cell clones and 3.3% of satellite progenitor clones contained mixed adipocytes and myotubes, supporting the notion that satellite cells are multipotent (Figure 1B, middle). The majority of satellite cell clones exclusively formed muscle-containing colonies (Figure

1B, right). These data demonstrate that satellite cells are multipotent and can clonally give rise to both myogenic and brown adipogenic cells.

Prdm16 Is Targeted by miR-133

We hypothesized that brown adipose determination of satellite cells is controlled by microRNAs, which regulate the expression of Prdm16 or other brown adipose determinants. Therefore, we performed whole-transcriptome RNA sequencing (RNA-Seq) for satellite cells and brown preadipocytes isolated from adult hindlimb muscles and interscapular BAT (iBAT), respectively, by established FACS schemes (Scimè et al., 2005) (Figure S2A). We identified 580 mRNAs and 88 microRNAs, which are differentially expressed between two cell lineages (Figures S2B and S2C, Table S1, and Table S2).

Satellite cell-enriched microRNAs and their predicted transcription factor targets enriched in brown preadipocytes were plotted to identify negative regulatory networks (Figure S2D). Analysis of the network suggested that Prdm16 is repressed by the satellite cell-enriched miR-133a and miR-133b. We identified a highly conserved target site for miR-133a and miR-133b with an absolutely conserved 8 nt seed sequence in the 3′UTR of *Prdm16* mRNA (Figure 2A). The conservation of the seed sequence suggests biological relevance of these microRNAs in regulating Prdm16 expression in humans.

We performed luciferase assays and RT-qPCR to investigate the direct targeting of *Prdm16* 3′UTR by miR-133. HEK293T cells transfected with reporter plasmids containing the *Prdm16* 3′UTRs showed markedly decreased luciferase activity and luciferase mRNA level in the presence of ectopic miR-133 (Figure 2B). Mutation of the conserved 8 nt seed sequence abrogated the miR-133-induced repression of the *Prdm16* 3′UTR. Similar results were also observed in C2C12 myoblasts (Figure S2E).

miR-133 belongs to a group of myomiRs, which are enriched in muscle tissue and myogenic cells (Chen et al., 2006; Williams et al., 2009). We confirmed the inverse expression patterns of Prdm16 and miR-133 in FACS-sorted BAT progenitors, satellite cell populations, and cultured primary myoblasts (Figure S2F). Thus, we hypothesized that direct targeting of Prdm16 by miR-133 represents a potential regulatory mechanism in brown adipose determination.

Overexpression of miR-133 Impairs Lineage Commitment of Brown Preadipocytes

Primary brown preadipocytes express low but evident levels of miR-133 (Walden et al., 2009). Therefore, we tested the effects of miR-133 overexpression on the brown adipose lineage fate of primary brown preadipocytes. To avoid “off-target” and “overloading” side effects, we utilized a lentivirus-based micro-RNA expression system to elevate the endogenous levels of miR-133 in primary brown preadipocytes within a physiological range.

Lentiviral overexpression of miR-133 resulted in markedly reduced protein levels of Prdm16 and Pgc1-α, which is a Prdm16 target and critical for BAT-specific thermogenic gene expression (Seale et al., 2007) (Figure 2C). Moreover, overexpression of miR-133 strongly impaired adipogenic differentiation of brown preadipocytes at confluent density, as evidenced by reduced number of ORO^{pos} adipocytes in the differentiation cultures (Figure 2D).

We further performed RT-qPCR to investigate gene expression signatures associated with lineage commitment of brown preadipocytes in response to miR-133 overexpression or repression (Figure 2E). Overexpression of miR-133 decreased the expression of brown adipogenic markers (*Prdm16, Pgc1a, Ucp1, Cidea*, and *miR-196a*) as well as genes associated with general adipogenesis (*Pparg, Fabp4, Cebpb*, and *Adipoq*). Notably,

overexpression of miR-133 led to markedly increased expression levels of myogenic transcription factors, *Pax7, MyoD*, and *Myogenin* as well as a myogenic differentiation marker, *myosin heavy chain 2* (*MyHC*). A white adipocyte-specific marker, *Leptin*, was also increased in miR-133 overexpression culture. By contrast, inhibition of miR-133 enhanced brown adipogenic commitment and differentiation, as evidenced by increased expression of *Prdm16, Pgc1a, Ucp1, Cidea, Pparg, Cebpb*, and *Adipoq*, as well as decreased expression of *Pax7, MyoD, Myogenin*, and *MyHC* (Figure 2E). These data indicate that miR-133 regulates brown adipose determination in primary brown preadipocytes by targeting Prdm16.

miR-133 Prevents Brown Adipose Determination in Satellite Cells

To investigate whether knockdown of miR-133 promotes brown adipose determination, we transfected satellite cells embedded within individual myofibers with mixtures of either antisense oligonucleotide (ASO) inhibitors or mimetics for miR-133a and miR-133b (>300 myofibers per treatment group) (Figure S3A). Remarkably, inhibition of miR-133 resulted in a pronounced increase of brown adipocytes in the culture, characterized by their nuclear Prdm16 staining and presence of oil droplets (Figure S3B, right). Conversely, no brown adipocytes were observed in myofiber cultures transfected with miR-133 mimetics (Figure S3B, middle).

To confirm that these brown adipocytes were derived from satellite cells, tdTomato-labeled satellite cells on myofibers isolated from *Pax7-CreER;R26R-tdTomato* mice (>300 myofibers per treatment group) were transfected with miR-133 ASO inhibitors (Figure 3A). Notably, we observed a dramatic 16-fold increase in the number of satellite cell-derived brown adipocytes (SC_BA), as evidenced by their Ucp1 and tdTomato double staining in response to miR-133 inhibition (Figure 3A). Thus, we conclude that miR-133 inhibition in satellite cells is sufficient to induce brown adipose determination.

The molecular nature of SC_BA was characterized following their enrichment by centrifugation based on their low density. After centrifugation, the supernatant fraction was enriched for SC_BA, whereas the pellet fraction was enriched for myotubes. The gene expression profiles of these SC_BA and myotube fractions were then compared with those of cultured differentiated brown preadipocytes originally also isolated from *Pax7-CreER;R26R-tdTomato* mice (Figure 3B). RT-qPCR revealed that the SC_BA-enriched supernatant fraction contained comparable levels of *tdTomato* mRNA relative to the myotube-enriched pellet fraction, consistent with the common satellite cell origin of these two types of cells. By contrast, the preadipocyte-derived brown adipocytes did not express *tdTomato*, confirming that Pax7 was not expressed in iBAT during tamoxifen induction. Intriguingly, SC_BA expressed a high level of *Ucp1* but less *Prdm16* relative to brown adipocytes, suggesting that a low level of Prdm16 is sufficient to support brown adipocyte determination in vitro. Consistent with miR-133 inhibitor treatment, SC_BA contained lower *miR-133* levels relative to brown adipocytes. As expected, the myotube fraction was enriched for *miR-133, Pax7*, and *MyHC* yet devoid of *Ucp1* mRNA. Taken together, these data support the hypothesis that miR-133 expression enforces myogenic commitment of satellite cells by targeting Prdm16 expression and repressing brown adipogenic determination.

We next investigated whether miR-133 represses brown adipose determination by targeting genes in addition to Prdm16. To address this question, we transiently expressed ectopic miR-133 in C3H10T1/2 mesenchymal progenitors in the absence or presence of ectopic Prdm16 lacking its 3′UTR (Prdm16_CDS) during the adipogenic determination stage (before adipogenic induction). In this manner, we could assess whether miR-133 targets any

other brown adipogenic determinants during adipogenic determination, whose repression cannot be rescued by Prdm16 ectopic expression (Figure S3C).

In the absence of Prdm16, ectopic expression of miR-133 moderately compromised the white adipose determination and differentiation of C3H10T1/2 progenitors, as evidenced by reduced Perilipin A expression combined with lack of Prdm16 or Ucp1 expression (Figures S3D and S3E). On the other hand, ectopic expression of Prdm16 markedly promoted brown adipose determination and differentiation, as evidenced by increased Perilipin A expression combined with strong induction of Ucp1 and Pgc1α. Critically, ectopic expression of miR-133 together with Prdm16 led to a comparable, if not improved, brown adipocyte phenotype as compared to Prdm16 overexpression alone. In addition, overexpression of miR-133 alone in C3H10T1/2 progenitors appeared not to induce myogenic determination as observed from brown preadipocyte cultures (Figure S3E, MyHC panel). These findings are consistent with the absence of miR-133 seed sequence in the 3′UTRs of *Pparg, Pgc1a/b, Cebpa/b/d*, and *Ucp1*. Therefore, we conclude that miR-133 prevents brown adipose determination by primarily targeting Prdm16.

Antagonism of miR-133 Induces Brown Adipose Determination of Satellite Cells during Muscle Regeneration

To investigate miR-133 function in brown adipose determination of satellite cells in vivo, we synthesized miR-133 antagomiR (miR-133 ASO) with an antisense sequence to both miR-133a and miR-133b, as well as a control “antagomiR” (control ASO) with the same chemical modifications and not antisense to any mouse gene or EST sequence (see the Experimental Procedures). We performed lineage tracing to distinguish effects of miR-133 ASO on satellite cells versus other cell types. Six-week-old *Pax7-CreER;R26R-tdTomato* mice were treated with tamoxifin as before (five consecutive daily injections), then aged to 10 weeks of age prior to initiating the experiment. Control ASO versus miR-133 ASO were injected into tibialis anterior (TA) muscles 3 days following saline injection (quiescent state) or cardiotoxin injection (to induce satellite cell activation) (Figure S4A). After 1 month, RT-qPCR was performed using RNA isolated from several tissues to evaluate the efficacy and scope of miR-133 ASO administration.

We detected striking reduction of both miR-133a and miR-133b expression within the TA muscles administrated with miR-133 ASO, with more prominent effects observed in resting muscles injected with miR-133 ASO (Figure 4A). In fact, miR-133 ASO injected into resting muscles also repressed miR-133a/b expression in the contralateral TA muscles, suggesting diffusion of this antagomiR under this condition. Such a “leaking” effect was not present when miR-133 ASO was injected into regenerating muscles. Notably, miR-133 expression in the myocardium was unaffected by the intramuscular administration of miR-133 ASO. In addition, miR-133 ASO had no effect on *let-7a* microRNA expression, confirming its specificity. Accordingly, we detected increased *Ucp1* mRNA within miR-133 ASO-injected regenerating muscle, yet not within other tissues or miR-133 ASO-injected resting muscle (Figure 4A). Similar repression of *miR-133a/b* and induction of *Ucp1* mRNA were detected after 3 months of a single miR-133 ASO injection in regenerating muscle, indicating long-lasting effects of this ASO in muscle (Figure S4B). Corroborating the RT-qPCR results, Ucp1 protein was specifically detected by immunoblotting of extracts from regenerated TA muscles that had received miR-133 ASO, but not in contralateral muscles or under other conditions (Figure 4B and Figure S4C). By comparison, Ucp3, a muscle abundant uncoupling protein, was largely unaffected by miR-133 ASO administration (Figure 4B). miR-133 ASO treatment following frozen injury-induced muscle regeneration similarly induced *Ucp1* mRNA level in treated TA muscle (Figure S4D).

To investigate whether miR-133 ASO was inducing satellite cells to undergo brown adipose determination in vivo, we performed immunofluorescence microscopy on cross-sections prepared from regenerating TA muscles treated with control- or miR-133 ASO (Figures 4C and 4D). Staining for Ucp1 and basal lamina-located Laminin confirmed Ucp1 staining only within miR-133 ASO-treated regenerating muscles. Moreover, we found that Ucp1^{pos} cells were located within muscle interstitium, distinct from surrounding myofibers ensheathed within the basal lamina (Figure 4C). In addition, we observed that these interstitial cells were immunoreactive to Perilipin A and nuclear Prdm16 (Figure 4D). Most importantly, the majority of these induced brown adipocytes were also labeled with tdTomato, indicating that they were derived from Pax7-expressing satellite cells (Figures 4C and 4D).

We observed markedly increased numbers of interstitial cells (Figure S4E) and ORO-stained cells (Figure S4F) located between regenerating myofibers in response to miR-133 ASO treatment. ASO-treated muscles contained on average 15.6 Ucp1^{pos} brown adipocytes per section, of which 83.3% were derived from satellite cells (Figure S4G). Also, each cross-section of miR-133 ASO-treated muscle contained on average 31.6 Prdm16^{pos} cells, of which 76.8% were derived from satellite cells (Figure S4H). Presumably, this difference reflects the expression of Prdm16 in lineage-committed yet undifferentiated brown preadipocytes. The remaining ~20% tdTomato^{neg} brown adipocytes may originate from unlabeled satellite cells or from other cell sources (data not shown).

Small amounts of BAT have previously been reported to exist in hindlimb muscles of obesity-resistant *129S6/SvEvTac* mice, but not in obesity-prone *C57BL/6* mice (Almind et al., 2007). By immunoblotting, we detected ectopically induced Ucp1 protein expression in miR-133 ASO-treated muscles (2 months after treatment) of *C57BL/6* mice fed with either a regular diet (RD) or a high-fat diet (HFD) (Figure 5A). Consistently, we did not observe Ucp1 expression in either control ASO-treated muscles or contralateral resting muscles under either diet condition. H/E staining and Ucp1 immunohistochemistry further confirmed the efficacy of miR-133 ASO in inducing ectopic Ucp1^{pos} brown adipocytes within muscle interstitium of *C57BL/6* mice under both diet conditions (2 months after treatment) (Figure 5B).

miR-133 Antagonism Induces Metabolically Active Brown Adipocytes in Muscle

We next investigated whether miR-133 ASO-induced BAT in muscle is metabolic active and can function as authentic BAT. To quantify bioenergetic effects of miR-133 ASO-induced BAT in muscle, we performed high-resolution respirometry on TA muscles after 2 months of either control or miR-133 ASO treatment (*C57BL/6* males fed on RD, n = 6 in each treatment group). We applied a two-step protocol that was specifically designed to reveal the metabolic functions of relatively rare BAT embedded within skeletal muscle (see the Supplemental Experimental Procedures). Compared to skeletal muscle, brown adipocytes have conspicuously higher uncoupled respiration rates particularly in response to fatty acids (FAs), which is due to their characteristic expression of mitochondrial Ucp1 (Cannon and Nedergaard, 2004). Thus, we first followed a well-established protocol to measure FA-induced uncoupled respiration in intact (nonpermeabilized) muscle preparations (Figure 5C) (Chance and Williams, 1955). We found that titration of octanoyl carnitine (a medium-chain FA covalently linked to carnitine, which can enter freely into intact cells and also into mitochrondrion via acylcarnitine translocase [Houten and Wanders, 2010]) increased mitochondrial respiration rate to 13.5 ± 1 pmol·s^{-1}·mg^{-1} in miR-133 ASO-treated TA muscle compared to 7.7 ± 1 pmol·s^{-1}·mg^{-1} in control (Figure 5D, uncoupled/intact cells). This marked difference in the response to FAs is highly consistent with reported acute activation of mitochondrial respiration rates in brown adipocytes exposed to FAs (Matthias et al., 2000).

We next sought to test whether this 1.75-fold increase in the respiration rate was due to potential changes in muscle cells. If these changes indeed occurred, we expected to detect similar increased lipid oxidative phosphorylation capacity in permeabilized muscle preparations (permeabilization allows various substrates to pass through the cell membrane; see the Supplemental Experimental Procedures). We measured maximal electron flow through electron-transferring flavoprotein (ETF) in a separate portion of TA muscles in the presence of ADP. In response to ADP, the lipid oxidative phosphorylation capacity was 13.0 ± 1 pmol·s^{-1}·mg^{-1} in the control muscle as compared to 13.8 ± 3 pmol·s^{-1}·mg^{-1} in the miR-133 ASO-treated muscles (Figure 5D, ETF/permeabilized cells). This observation strongly supports the notion that the higher respiration rate in intact miR-133 ASO-treated muscle is due to FA-induced uncoupling in brown adipocytes, not in muscle cells. Therefore, we estimate that the induction of uncoupling respiration by miR-133 ASO leads to an additional 0.3 cal·hr^{-1}·mg^{-1} of energy expenditure in the treated TA muscle.

To further investigate possible bioenergetic effects of miR-133 ASO on muscle cells, we compared coupled state 3 respiration rates in treated and control permeabilized muscle tissues under full electron supply through complexes I and II (Figure 5D, permeabilized cells). No difference in electron transport through complex I (NADH dehydrogenase) between control and treated muscles was observed after electron transport through ETF was inhibited by the titration of glutamate (treated = 33 ± 3 pmol·s^{-1}·mg^{-1}, control = 28 ± 2 pmol·s^{-1}·mg^{-1}, p = 0.2). Maximal cellular state 3 respiration or oxidative phosphorylation capacity (P_{I+II}) was induced with the addition of succinate to provide additional electron flow through complex II (succinate dehydrogenase). This capacity reflects the maximal mitochondrial capacity to catalyze Redox reactions that are primarily coupled to the production of ATP via ATP synthase. Again, no difference in maximal coupled respiration between control and miR-133 ASO-treated muscles was observed (Figure 5D, P_{I+II}/ permeabilized cells). Similar results were derived from contralateral soleus muscles of control or miR-133 ASO-treated mice (Figure S5A). As both glutamate and succinate are poor substrates for BAT mitochondria (Cannon and Nedergaard, 2001), these results rule out any significant bioenergetic effect of miR-133 ASO on skeletal muscle cells.

Altogether, these data support the assertion that miR-133 ASO treatment in regenerating muscle results in unaltered coupled respiration in treated muscle cells but elicits drastic increases in uncoupled respiration, presumably owing to ectopically induced brown adipocytes within the muscle interstitium.

Metabolically active BAT has been identified in adult human by [^{18}F]-fluorodeoxyglucose positron emission tomography ([^{18}F]-FDG PET), due to dramatic glucose uptake by this tissue after sympathetic activation (Nedergaard et al., 2007). To visualize active BAT within muscle, we performed [^{18}F]-FDG PET imaging on control or miR-133 ASO-treated mice (n = 5 for 133 ASO-treated mice, n = 4 for control-treated muscle; 2 months after treatment) after acute sympathetic activation by selective β3-adrenergic receptor agonist, CL316,243. We observed a dramatic increase of FDG uptake in miR-133 ASO-treated TA muscles compared to contralateral TA muscles or TA muscles within control ASO-treated mice (Figure 5E and Figure S5B). To rule out possible direct and indirect effects of CL316,243 on glucose/FDG uptake by skeletal muscle cells, we normalized FDG activities derived from regions of interest (ROIs) of treated TA muscles to those of contralateral TA muscles (Figure 5F). On average, miR-133 ASO-treated TA muscles after CL316,243-stimulated sympathetic activation exhibited a 1.3-fold increase of glucose/FDG uptake compared to control, strongly arguing that the ectopic-induced brown adipocytes in miR-133 ASO-treated TA muscles are metabolically active upon activation. Such a drastic increase was not observed without the sympathetic activation preceding anesthesia (baseline). As a reference, glucose/FDG uptake by iBAT expectedly increased 2.3- to 2.5-fold after CL316,243-

stimulated sympathetic activation in both control and miR-133 ASO-treated mice (Figure 5F).

A hallmark of active brown adipocytes is their unique thermogenic capability via extensive uncoupled respiration in abundant mitochondria (Cannon and Nedergaard, 2004). Therefore, we directly assessed the thermogenic capability of muscle-embedded brown adipocytes by thermographic imaging of control- or miR-133 ASO-treated mice fed with either RD or HFD (n = 5 per treatment group per diet group; Figure 5G). We observed increased surface temperatures on miR-133 ASO-treated hindlimbs compared to contralateral hindlimbs or hindlimbs of control ASO-treated mice (Figure 5G). On average, the surface temperatures on miR-133 ASO-treated hindlimbs were 0.7°C or 0.9°C higher than control hindlimbs for mice fed with RD or HFD, respectively (Figure 5H). We observed no difference in expression of *IL-1β* and *TNF-α* between control and treated muscles, supporting the assertion that the temperature increase is not due to inflammation (Figure S5C).

Taken together, our data provide compelling evidence that the induced intramuscular BAT induced by miR-133 ASO treatment is metabolically active.

Antagonism of miR-133 during Muscle Regeneration Reduced Adiposity, Augmented Energy Expenditure, and Improved Glucose Tolerance

Intramuscular brown adipocytes have been described in *129S6/SvEvTac* mice and in $Lxr^{-/-}$ mice (deficient for Liver X receptors), both of which display increased energy expenditure and resistance to obesity (Almind et al., 2007; Kalaany et al., 2005). We therefore assessed systematic metabolic consequences of miR-133 ASO treatment in regenerating TA muscle.

Treated and control *C57BL/6* male mice were raised on either RD or HFD in individual cages at 22°C (n = 5 per treatment per diet group). In both diet groups, miR-133 ASO-treated mice were obviously leaner than the control mice at 4 months after treatment (Figure 6A). Quantitatively, miR-133 ASO-treated mice displayed reduced gain in body weight over the 4 month period after ASO administration (Figure 6B). Close examination revealed significant reduction of weights in inguinal white fat depots (igWAT) and epididymal white fat depots (epiWAT), yet the mass of iBAT depots and treated TA muscles was unaffected (Figure S6A).

To assess whether miR-133 ASO treatment leads to increased whole-body energy expenditure, we carried out indirect calorimetry studies at 2–3 months after ASO treatment on control and miR-133 ASO-treated mice (*C57BL/6*, male, individually caged, n = 5 per treatment group per diet group; Figure 6C and Figure S6B). We detected a significant increase of total energy expenditure in miR-133 ASO-treated mice during light cycle (Figure 6C, left) without change in physical activities (Figure 6D, left). Intriguingly, this amount of energy expenditure is coincident with the increase of mitochondrial respirometry-measured energy expenditure in miR-133 ASO-treated TA muscles after adjustment with TA muscle mass (Figure S6A; 0.3 $cal \cdot hr^{-1} \cdot mg^{-1} \times 75$ mg = 0.0225 $kcal \cdot hr^{-1}$). Thus, we reasoned that increased uncoupled respiration due to ectopically induced intramuscular BAT likely contributes significantly to the total energy expenditure increase in light cycle. In dark cycle (when mice are active and feeding), the energy expenditure is conspicuously high in miR-133 ASO-treated mice (Figure 6C, right), which is associated with increased physical activities for the mice during the dark cycle (Figure 6D, right).

Similarly, we detected significantly increased total energy expenditure in miR-133 ASO-treated mice fed the HFD during light cycle (Figure S6B, left), without a difference in physical activities (Figure S6C, left). No significant increase in energy expenditure or physical activity was recorded in these mice over the dark cycle when compared to control

mice (Figures S6B and S6C, right panels). This discrepancy may be related to the abnormally low respiratory exchange ratio (~0.76) in the control mice fed with HFD (Figure S6D), which indicates an increased proportion of lipid oxidation in the control mice. The 24 hr food intake in miR-133 ASO-treated mice was comparable to that of control mice for both diet groups (Figure S6E), suggesting the reduction of body weight is likely due to the enhanced thermogenesis, and hence lower food efficiency, in the mice. Intriguingly, miR-133 ASO treatment also led to much improved glucose tolerance in both diet groups (Figure 6E and Figure S6F). In addition, H/E staining and microscopy of tissue sections from fat depots and liver revealed that miR-133 ASO-treated mice exhibited reduced numbers of infiltrating inflammatory cells in epi-WAT and reduced liver steatosis when fed the HFD (Figure S6G). Notably, the body weight and glucose tolerance status of our control mice resemble those of *C57BL/6* mice (in the same age) reported in numerous studies, which argues that the beneficial effects of miR-133 ASO treatment was not due to any cryptic effect of our control antagomiR.

Therefore, we conclude that miR-133 antagonism by ASO injection during muscle regeneration elicits profound changes in energy metabolism at the whole-body level, consistent with a leaner and healthier phenotype.

The Expression of miR-133 Is Downregulated In Skeletal Muscles after Cold Exposure, which Is Coincident with Emergence of Satellite Cell-Derived Brown Adipocytes

We next investigated whether the brown adipose determination of satellite cells occurs under physiological conditions that downregulate miR-133 expression. It has been reported that chronic cold exposure induces Ucp-1^{pos} adipocytes (“brite” or “beige” adipocytes), which morphologically resemble brown adipocytes yet arise from a non-Myf5 cell lineage, in subcutaneous WAT (Frontini and Cinti, 2010; Seale et al., 2011). We performed RT-qPCR using RNA isolated from multiple adipose and muscle tissues to evaluate the expression of miR-133 and BAT markers (Prdm16 and Ucp1) in response to cold exposure (1 week at 4°C; Figure 7A). We found cold exposure represses the expression of miR-133 in all investigated skeletal muscle tissues and brown/white adipose tissues. Coincidently, induced brown adipose determination/differentiation (as evidenced by increased *Prdm16* and *Ucp1* mRNA levels) was also observed in subcutaneous WAT depots and chunk muscles (e.g., intercostal muscles, back muscles, and paraspinal muscles), but not limb muscles (e.g., tibialis anterior).

To confirm satellite cell-derived brown adipocytes were induced by cold exposure, we performed immunofluorescence microscopy on cross-sections prepared from paraspinal muscles of cold-exposed *Pax7-CreER;R26R-tdTomato* mice. Strikingly, we observed emerging tdTomato^{pos}, Ucp1^{pos} adipocytes located within the interstitium of paraspinal muscles after cold exposure (Figure 7B). Such adipocytes were not detected in paraspinal muscles of the control *Pax7-CreER;R26R-tdTomato* mice raised under room temperature (23°C). Therefore, our observations implicate miR-133 in the physiological regulation of brown adipose determination of satellite cells in response to cold exposure.

DISCUSSION

Using lineage tracing and clonal analysis, we found that satellite cells in adult muscle are bona fide bipotential stem cells that can give rise to brown adipogenic as well as myogenic progenitors. We also identified a microRNA expressed in satellite cells and upregulated as the myogenic program progresses—miR-133—that directly represses the expression of Prdm16 to enforce myogenic commitment in satellite cells. Thus miR-133 functions as a switch to regulate the lineage choice between brown adipogenic versus myogenic determination.

We demonstrated that antagonizing miR-133 function by anti-sense oligos (antagomiR) in activated satellite cells in response to muscle injury resulted in the efficient induction of brown adipocytes within the muscle interstitium. We estimate that each treated TA muscle would contain tens of thousands of brown adipocytes based on enumeration of these cells as well as Ucp1 protein levels (Figure 4). Notably, the stimulatory effect of miR-133 ASO on brown adipose determination likely occurs in the early stage of muscle regeneration (within 2 weeks after muscle injury). Thus, satellite cell-derived brown adipocytes, once formed, do not require constant exposure to miR-133 ASO to maintain their function. The targeting specificity of miR-133 ASO argues for a pivotal role of miR-133 in BAT determination in muscle. However, it should also be noted that miR-133 may also target other biological processes in addition to de novo BAT formation in vivo. Future studies will reveal whether brown adipose determination of satellite cells occurs within muscles of miR-133 compound mutant mice (*miR-133a-1*$^{-/-}$; *miR-133a-2*$^{-/-}$; *miR-133b*$^{-/-}$).

We found that cold exposure represses the expression of miR-133 in multiple skeletal muscle tissues along with brown and white adipose tissues. Correspondingly, cold exposure also induced brown adipose determination/differentiation (as indicated by increased *Prdm16* and *Ucp1* mRNA levels) in subcutaneous WAT depots and trunk muscles. To explore whether the increased *Prdm16/Ucp1* expression in trunk muscles was due to induced satellite cell-derived brown adipocytes, we further exposed *Pax7-CreER;R26R-tdTomato* mice to cold and performed immunostaining (Figure S7B) on paraspinal muscle cross-sections. Strikingly, we observed satellite cell-derived brown adipocytes (tdTomato^{pos}, Ucp1^{pos}) located within paraspinal muscle interstitium. Recently, it was reported that miR-133 regulates Prdm16 in committed brown adipogenic cells, and cold treatment of cultured cells resulted in down-regulation of miR-133 and upregulation of Prdm16 and Ucp1 (Trajkovski et al., 2012). Taken together, these observations implicate regulation of miR-133 expression as a key thermo-regulatory mechanism in the whole-animal response to acute and chronic cold.

Our investigation of the metabolic phenotypes associated with miR-133 ASO-treated TA muscles/hindlimbs indicated that the induced brown adipocytes in the muscle interstitium are metabolically active (Figure 5). This notion is supported by bioenergetics results of miR-133 ASO-treated TA muscles in vitro, which showed markedly increased uncoupled respiration in nonpermeabilized miR-133 ASO-treated muscle in response to Ucp1 activation by FAs. This increased uncoupled respiration rate has potentially important implications for energy expenditure and weight control in vivo. The difference in uncoupled respiration between control and miR-133 ASO treatment TA muscles is equivalent to ~0.023 kcal·hr^{-1}, which would fully account for the measured difference of total energy expenditure between control and miR-133 ASO-treated mice in the light cycle and ~15% of the difference found in the dark cycle (when more energy is used to support coupled, ATP synthase-dependent respiration during physical activity).

Our experiments also demonstrate that miR-133 ASO induced brown adipocytes in muscle function in the same manner as authentic BAT, in terms of their energy uptake ([^{18}F]-FDG/glucose uptake; Figures 5E and 5F) and energy expenditure (thermogenesis; Figures 5G and 5H). It is noteworthy that the markedly increased glucose/FDG uptake in miR-133 ASO-treated muscles was only revealed after selective β3-adrenergic receptor activation (CL316,243). Importantly, β3-adrenergic receptors express abundantly on brown adipocytes but little on muscle cells (Krief et al., 1993).

Skeletal muscle is a compatible tissue for adaptive thermogenesis of resident brown adipocytes. It has been well established that skeletal muscle cells are indirectly controlled by the sympathetic nervous system via diffusible adrenergic transmitters released from

abundant vascular sympathetic innervations (Bowman and Nott, 1969). Thus, it is reasonable to speculate that interstitial satellite cell-derived brown adipocytes would be readily accessed by catecholamines from the vasculature relative to myofibers surrounded by basal lamina. The elevated glucose/FDG uptake in response to CL316,243 strongly implicates the presence of β3-adrenergic receptors on satellite cell-derived brown adipocytes.

Skeletal muscle has a very high metabolic capacity. Therefore, it is intriguing to hypothesize that the activation of muscle-embedded BAT may parallel sympathetic activation and dynamic regulation of oxygen/energy source supply via vasodilatation in response to need for muscle motor output. Indeed, the obesity resistance trait of *129S6/SvEvTac* mice has been attributed to ectopic intramuscular BAT, which appeared to be more sensitive to adrenergic agonists in Ucp1 induction as compared to iBAT (Almind et al., 2007). Similar to *129S6/SvEvTac* mice, obesity-prone *C57BL/6* mice showed reduced adiposity, augmented energy expenditure, and improved whole-body insulin sensitivity in response to miR-133 ASO treatment and BAT induction in muscle (Figure 6). These systemic effects of miR-133 ASO may associate with direct effects of ectopically induced satellite cell-derived brown adipocytes in muscle, or alternatively ensue from indirect effects from reduced body weight and adiposity (e.g., increased muscle insulin sensitivity may result from reduced adiposity or increased physical activity).

The data from mitochondrial respirometry clearly indicate that neither miR-133 ASO-treated TA muscles nor the contralateral soleus muscles have significantly increased oxidative phosphorylation capacity compared to the control muscles (Figure 5D and Figure S5A). The isolated activities of cytochrome oxidase in the contralateral soleus muscles, a marker for mitochondrial content (Larsen et al., 2012), were also comparable between treatment groups (miR-133 ASO treated, 130 ± 13 $pmol \cdot s^{-1} \cdot mg^{-1}$; control ASO treated, 113 ± 24 $pmol \cdot s^{-1} \cdot mg^{-1}$, $p = 0.5$). These results indicate that the miR-133 ASO treatment regime does not mimic a “training” effect in skeletal muscle cells. Further investigation may shed light on the cause(s) of increased physical activity levels in miR-133 ASO-treated mice. Nevertheless, the phenotypes linked with miR-133 ASO treatment evidently argue for positive influences of miR-133 ASO on metabolism.

Here, we demonstrate that satellite cells can differentiate into either myocytes or brown adipocytes. The lineage switch between myogenic and brown adipogenic commitment is controlled by myomiR miR-133, which is highly expressed in satellite cells. Functional brown adipocytes can be induced from satellite cells by inhibiting miR-133 function during muscle regeneration or by cold exposure accompanied with downregulation of miR-133 expression. Therefore, targeting miR-133 activity in adult muscle stem cells represents an attractive strategy to stimulate a physiological effective increase in the numbers of active brown adipocytes in vivo.

EXPERIMENTAL PROCEDURES

Induced Brown Adipocytes In Vivo by miR-133 AntagomiR

To induce brown adipocytes in vivo, 10 mg/mL cardiotoxin solution (50 μl) was intramuscularly injected into TA muscles of 10-week-old *Pax7-CreER/R26R-tdTomato* mice (Figure 4) or *C57BL/6* mice (Figure 5 and Figure 6). Alternatively, frozen injury was performed by applying liquid nitrogen-cooled tweezers tips directly onto the anterior sides of TA muscles (Figure S4H). After 3 days, 20 μg of miR-133 antagomiR or control antagomiR in saline (50 μl) was intramuscularly injected into the same injured TA muscles (on right hindlimbs). To test efficacy of miR-133 ASO in intact muscles, saline, instead of cardiotoxin, was injected to TA muscles before miR-133 ASO administration (Figures 4A

and 4B). miR-133 antagomiR and scramble antagomiR were designed as previously described (Krützfeldt et al., 2005).

miR-133 antagomiR sequence and modifications were as follows: 5′-*mA* mUmAmGmCmUmGmGmUmUmGmAmAmGmGmGmAmC*mC*mA*mA* mAChl-3′; scramble antagomiR sequence and modifications, 5′-*mA*mAmGm AmAmUmGmAmCmGmAmUmCmGmGmUmAmGmG*mG*mC*mA*mCChl-3′. “m” represents a 2′-O-methyl-modified nucleotide. Asterisk indicates a phosphorothioate linkage. “Chl” denotes a 3′ cholesterol moiety.

Indirect Calorimetry

Whole-body O_2 consumption and CO_2 production were measured using an open-circuit four-chamber indirect calorimetry system with automatic temperature and light controls (Columbus Instruments). Physical activities during indirect calorimetry were measured using infrared laser beam sets. Mice had access ad libitum to food and water in respiration chambers. Data were recorded for a 24 hr period with light between 06:00 and 18:00.

[^{18}F]-FDG PET Imaging and X-ray Computed Tomography

All animal procedures comply with the Canadian Council on Animal Care’s Guide to the Care and Use of Experimental Animals, the Animals for Research Act, and were approved by the Animal Care Committee at University of Ottawa. Mouse PET imaging was performed with an Inveon PET scanner (Siemens Preclinical Solutions, Knoxville, TN, USA). Control or miR-133 ASO-treated *C57BL/6* male mice fed with regular diet were anesthetized under 2% isoflurane. Mice were administrated with ~1 mCi [^{18}F] fluoro-2-deoxyglucose ([^{18}F] FDG) via tail vein injection and subjected to an 80 min dynamic scan. Data analysis was performed using the Inveon Research Workplace software to determine the standardized uptake values (SUVs) (activity concentration/injected dose × body weight) based on drawn ROIs at the end of the 80 min scanning period. Computed tomography (CT) with hindlimbs centered in the field of view was performed before the microPET imaging. Reconstructed CT images were registered with microPET images to precisely identify TA muscles on hindlimbs. To activate brown adipocytes, a β3-adrenergic selective agonist, CL-316,243, was administrated (1 mg/kg body weight; i.p. injection) 20 min before the anesthesia.

Thermographic Imaging

Mouse thermographic imaging was performed with a FLIR T640 infrared camera with highest sensitivity set to ~35°C. Control or miR-133 ASO-treated *C57BL/6* male mice fed with either a regular diet or a HFD were shaved at both of the hindlimbs 1 day before the imaging. Subject mice were quickly anesthetized under ~1% isoflurane, and thermographic images were taken immediately after the mice were anesthetized (within 2 min). Data analysis was performed using FLIR QuickReport software with measuring crosses set on the TA muscle areas on lower hindlimbs and the neck areas.

Statistical Analysis

Error bars are SEM. Asterisk indicates significant pairwise comparison by t test, *$p \leq 0.05$, **$p \leq 0.01$, ***$p \leq 0.001$.

Supplementary Material

Refer to Web version on PubMed Central for supplementary material.

Acknowledgments

We thank Brianne Thrush for help on high-resolution respirometry, Christine Archer for help on microPET/CT imaging, Céline Aguer and Jian Xuan for help on indirect calorimetry, Paul Oleynick for fluorescent-activated cell sorting, and Jennifer Ritchie for animal husbandry. H.Y. was supported by fellowships from Canadian Institutes of Health Research (CIHR), CIHR Training Program in Regenerative Medicine, and the Ontario Research Fund. M.A.R. holds the Canada Research Chair in Molecular Genetics. This work was funded by the Canadian Institutes of Health Research grant MOP81288, NIH/NIAMS grant R01AR044031, and Ontario Research Fund grants (to M.A.R.), and by EuTRACC, a European Commission 6th Framework grant (to F.G.). H.Y., R.B., M-E.H., and M.A.R. conceived of and designed experiments, and prepared the manuscript. H.Y. executed most of the experiments and performed bioinformatic analyses. A.P. executed experiments in Figure 1 and Figure S3B. V.D.S. prepared retroviruses. C.F.B. executed experiments in Figures S4F and S4G. G.A. helped on experiments in Figures 5C and 5D and Figure S5A. P.S. provided anti-Prdm16 antibody. S.T., P.F., and R.A.D. designed experiments and analyzed data in Figures 5E and 5F and Figure S5B. W.v.I. and F.G. provided support to high-throughput sequencing of satellite cell transcriptome. R.B. designed and performed experiments and analyzed data in Figures 5C and 5D and Figure S5A.

References

Almind K, Manieri M, Sivitz WI, Cinti S, Kahn CR. Ectopic brown adipose tissue in muscle provides a mechanism for differences in risk of metabolic syndrome in mice. Proc Natl Acad Sci USA. 2007; 104:2366–2371. [PubMed: 17283342]

Atit R, Sgaier SK, Mohamed OA, Taketo MM, Dufort D, Joyner AL, Niswander L, Conlon RA. Beta-catenin activation is necessary and sufficient to specify the dorsal dermal fate in the mouse. Dev Biol. 2006; 296:164–176. [PubMed: 16730693]

Bosnakovski D, Xu Z, Li W, Thet S, Cleaver O, Perlingeiro RC, Kyba M. Prospective isolation of skeletal muscle stem cells with a Pax7 reporter. Stem Cells. 2008; 26:3194–3204. [PubMed: 18802040]

Bowman WC, Nott MW. Actions of sympathomimetic amines and their antagonists on skeletal muscle. Pharmacol Rev. 1969; 21:27–72. [PubMed: 4304935]

Cannon B, Nedergaard J. Respiratory and thermogenic capacities of cells and mitochondria from brown and white adipose tissue. Methods Mol Biol. 2001; 155:295–303. [PubMed: 11293080]

Cannon B, Nedergaard J. Brown adipose tissue: function and physiological significance. Physiol Rev. 2004; 84:277–359. [PubMed: 14715917]

Chance B, Williams GR. A simple and rapid assay of oxidative phosphorylation. Nature. 1955; 175:1120–1121. [PubMed: 14394122]

Chargé SB, Rudnicki MA. Cellular and molecular regulation of muscle regeneration. Physiol Rev. 2004; 84:209–238. [PubMed: 14715915]

Chen JF, Mandel EM, Thomson JM, Wu Q, Callis TE, Hammond SM, Conlon FL, Wang DZ. The role of microRNA-1 and microRNA-133 in skeletal muscle proliferation and differentiation. Nat Genet. 2006; 38:228–233. [PubMed: 16380711]

Cypess AM, Kahn CR. Brown fat as a therapy for obesity and diabetes. Curr Opin Endocrinol Diabetes Obes. 2010; 17:143–149. [PubMed: 20160646]

Cypess AM, Lehman S, Williams G, Tal I, Rodman D, Goldfine AB, Kuo FC, Palmer EL, Tseng YH, Doria A, et al. Identification and importance of brown adipose tissue in adult humans. N Engl J Med. 2009; 360:1509–1517. [PubMed: 19357406]

Frontini A, Cinti S. Distribution and development of brown adipocytes in the murine and human adipose organ. Cell Metab. 2010; 11:253–256. [PubMed: 20374956]

Ghorbani M, Himms-Hagen J. Appearance of brown adipocytes in white adipose tissue during CL 316,243-induced reversal of obesity and diabetes in Zucker fa/fa rats. Int J Obes Relat Metab Disord. 1997; 21:465–475. [PubMed: 9192230]

Houten SM, Wanders RJ. A general introduction to the biochemistry of mitochondrial fatty acid β-oxidation. J Inherit Metab Dis. 2010; 33:469–477. [PubMed: 20195903]

Joe AW, Yi L, Natarajan A, Le Grand F, So L, Wang J, Rudnicki MA, Rossi FM. Muscle injury activates resident fibro/adipogenic progenitors that facilitate myogenesis. Nat Cell Biol. 2010; 12:153–163. [PubMed: 20081841]

Kajimura S, Seale P, Tomaru T, Erdjument-Bromage H, Cooper MP, Ruas JL, Chin S, Tempst P, Lazar MA, Spiegelman BM. Regulation of the brown and white fat gene programs through a PRDM16/CtBP transcriptional complex. Genes Dev. 2008; 22:1397–1409. [PubMed: 18483224]

Kalaany NY, Gauthier KC, Zavacki AM, Mammen PP, Kitazume T, Peterson JA, Horton JD, Garry DJ, Bianco AC, Mangelsdorf DJ. LXRs regulate the balance between fat storage and oxidation. Cell Metab. 2005; 1:231–244. [PubMed: 16054068]

Kopecky J, Clarke G, Enerbäck S, Spiegelman B, Kozak LP. Expression of the mitochondrial uncoupling protein gene from the aP2 gene promoter prevents genetic obesity. J Clin Invest. 1995; 96:2914–2923. [PubMed: 8675663]

Krief S, Lönnqvist F, Raimbault S, Baude B, Van Spronsen A, Arner P, Strosberg AD, Ricquier D, Emorine LJ. Tissue distribution of beta 3-adrenergic receptor mRNA in man. J Clin Invest. 1993; 91:344–349. [PubMed: 8380813]

Krützfeldt J, Rajewsky N, Braich R, Rajeev KG, Tuschl T, Manoharan M, Stoffel M. Silencing of microRNAs in vivo with 'antagomirs'. Nature. 2005; 438:685–689. [PubMed: 16258535]

Kuang S, Kuroda K, Le Grand F, Rudnicki MA. Asymmetric self-renewal and commitment of satellite stem cells in muscle. Cell. 2007; 129:999–1010. [PubMed: 17540178]

Larsen S, Nielsen J, Hansen CN, Nielsen LB, Wibrand F, Stride N, Schroder HD, Boushel R, Helge JW, Dela F, Hey-Mogensen M. Biomarkers of mitochondrial content in skeletal muscle of healthy young human subjects. J Physiol. 2012; 590:3349–3360. [PubMed: 22586215]

Lepper C, Fan CM. Inducible lineage tracing of Pax7-descendant cells reveals embryonic origin of adult satellite cells. Genesis. 2010; 48:424–436. [PubMed: 20641127]

Matthias A, Ohlson KB, Fredriksson JM, Jacobsson A, Nedergaard J, Cannon B. Thermogenic responses in brown fat cells are fully UCP1-dependent. UCP2 or UCP3 do not substitute for UCP1 in adrenergically or fatty scid-induced thermogenesis. J Biol Chem. 2000; 275:25073–25081. [PubMed: 10825155]

Nedergaard J, Bengtsson T, Cannon B. Unexpected evidence for active brown adipose tissue in adult humans. Am J Physiol Endocrinol Metab. 2007; 293:E444–E452. [PubMed: 17473055]

Nedergaard J, Bengtsson T, Cannon B. Three years with adult human brown adipose tissue. Ann N Y Acad Sci. 2010; 1212:E20–E36. [PubMed: 21375707]

Nishijo K, Hosoyama T, Bjornson CR, Schaffer BS, Prajapati SI, Bahadur AN, Hansen MS, Blandford MC, McCleish AT, Rubin BP, et al. Biomarker system for studying muscle, stem cells, and cancer in vivo. FASEB J. 2009; 23:2681–2690. [PubMed: 19332644]

Ouellet V, Labbé SM, Blondin DP, Phoenix S, Guérin B, Haman F, Turcotte EE, Richard D, Carpentier AC. Brown adipose tissue oxidative metabolism contributes to energy expenditure during acute cold exposure in humans. J Clin Invest. 2012; 122:545–552. [PubMed: 22269323]

Pfannenberg C, Werner MK, Ripkens S, Stef I, Deckert A, Schmadl M, Reimold M, Häring HU, Claussen CD, Stefan N. Impact of age on the relationships of brown adipose tissue with sex and adiposity in humans. Diabetes. 2010; 59:1789–1793. [PubMed: 20357363]

Saito M, Okamatsu-Ogura Y, Matsushita M, Watanabe K, Yoneshiro T, Nio-Kobayashi J, Iwanaga T, Miyagawa M, Kameya T, Nakada K, et al. High incidence of metabolically active brown adipose tissue in healthy adult humans: effects of cold exposure and adiposity. Diabetes. 2009; 58:1526–1531. [PubMed: 19401428]

Scimè A, Grenier G, Huh MS, Gillespie MA, Bevilacqua L, Harper ME, Rudnicki MA. Rb and p107 regulate preadipocyte differentiation into white versus brown fat through repression of PGC-1alpha. Cell Metab. 2005; 2:283–295. [PubMed: 16271529]

Seale P, Sabourin LA, Girgis-Gabardo A, Mansouri A, Gruss P, Rudnicki MA. Pax7 is required for the specification of myogenic satellite cells. Cell. 2000; 102:777–786. [PubMed: 11030621]

Seale P, Kajimura S, Yang W, Chin S, Rohas LM, Uldry M, Tavernier G, Langin D, Spiegelman BM. Transcriptional control of brown fat determination by PRDM16. Cell Metab. 2007; 6:38–54. [PubMed: 17618855]

Seale P, Bjork B, Yang W, Kajimura S, Chin S, Kuang S, Scimè A, Devarakonda S, Conroe HM, Erdjument-Bromage H, et al. PRDM16 controls a brown fat/skeletal muscle switch. Nature. 2008; 454:961–967. [PubMed: 18719582]

Seale P, Conroe HM, Estall J, Kajimura S, Frontini A, Ishibashi J, Cohen P, Cinti S, Spiegelman BM. Prdm16 determines the thermogenic program of subcutaneous white adipose tissue in mice. J Clin Invest. 2011; 121:96–105. [PubMed: 21123942]

Trajkovski M, Ahmed K, Esau CC, Stoffel M. MyomiR-133 regulates brown fat differentiation through Prdm16. Nat Cell Biol. 2012; 14:1330–1335. [PubMed: 23143398]

van Marken Lichtenbelt WD, Vanhommerig JW, Smulders NM, Drossaerts JM, Kemerink GJ, Bouvy ND, Schrauwen P, Teule GJ. Cold-activated brown adipose tissue in healthy men. N Engl J Med. 2009; 360:1500–1508. [PubMed: 19357405]

Virtanen KA, Lidell ME, Orava J, Heglind M, Westergren R, Niemi T, Taittonen M, Laine J, Savisto NJ, Enerbäck S, Nuutila P. Functional brown adipose tissue in healthy adults. N Engl J Med. 2009; 360:1518–1525. [PubMed: 19357407]

Walden TB, Timmons JA, Keller P, Nedergaard J, Cannon B. Distinct expression of muscle-specific microRNAs (myomirs) in brown adipocytes. J Cell Physiol. 2009; 218:444–449. [PubMed: 18937285]

Wang YX, Rudnicki MA. Satellite cells, the engines of muscle repair. Nat Rev Mol Cell Biol. 2012; 13:127–133. [PubMed: 22186952]

Williams AH, Liu N, van Rooij E, Olson EN. MicroRNA control of muscle development and disease. Curr Opin Cell Biol. 2009; 21:461–469. [PubMed: 19278845]

Zingaretti MC, Crosta F, Vitali A, Guerrieri M, Frontini A, Cannon B, Nedergaard J, Cinti S. The presence of UCP1 demonstrates that metabolically active adipose tissue in the neck of adult humans truly represents brown adipose tissue. FASEB J. 2009; 23:3113–3120. [PubMed: 19417078]

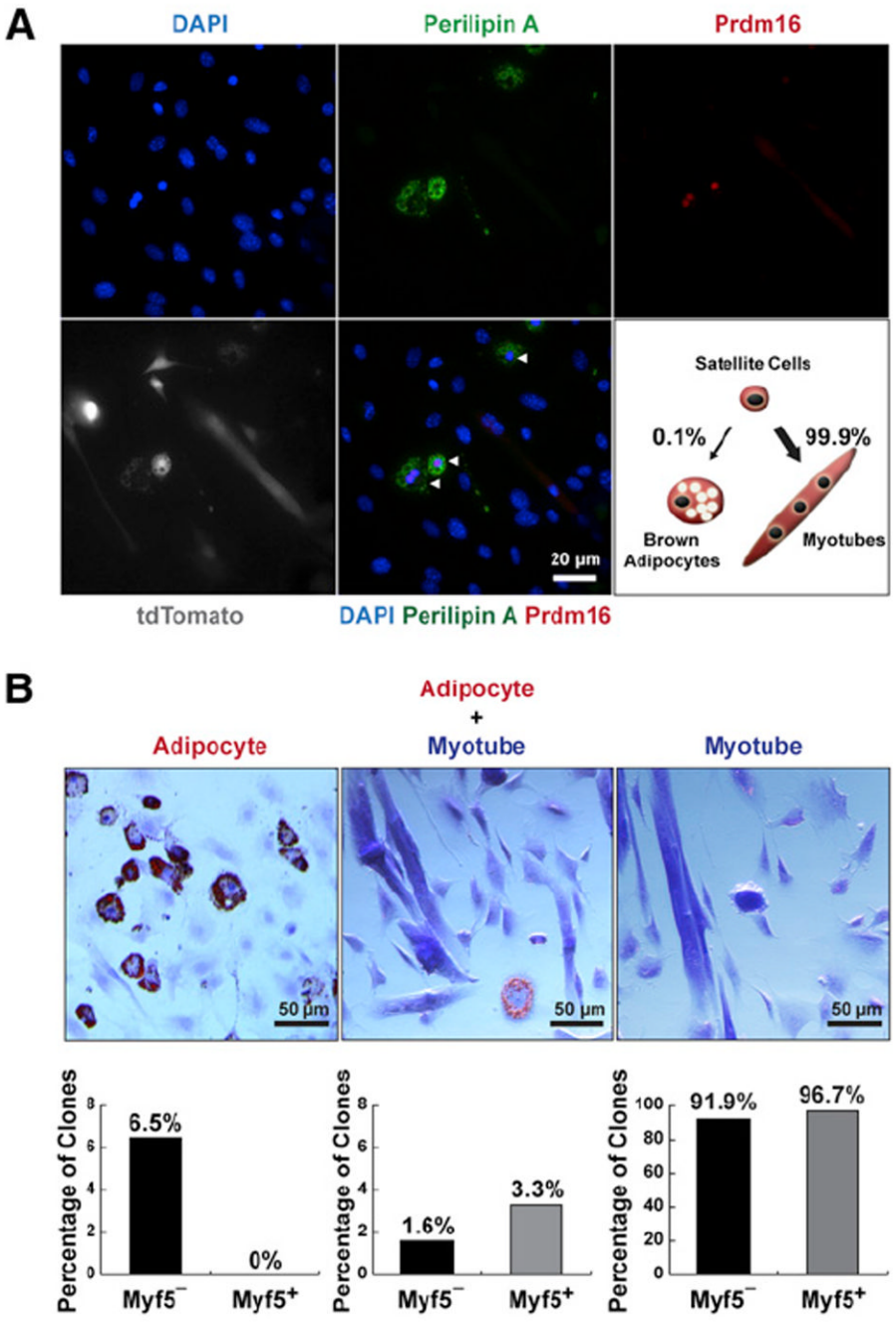

Figure 1. Satellite Cells Differentiate into Brown Adipocytes

(A) Satellite cells differentiated into brown adipocytes (arrowheads) in myofiber cultures under proadipogenic conditions. Myofibers (n > 600) with resident satellite cells were isolated from *Pax7-CreER/R26R-tdTomato* EDL muscles and cultured for 12 days in proadipogenic medium. Lineage-marked satellite cell-derived brown adipocytes expressed tdTomato and Prdm16, Perilipin A.

(B) Clonal analysis of FACS-isolated single satellite stem cells and satellite myogenic progenitors (n > 2,000 for each cell type) indicates some satellite cells are bipotential. Approximately 1.6% of satellite stem cells and 3.3% satellite myogenic progenitors gave rise to mixed muscle and adipocyte-containing colonies. In addition, 6.5% of satellite stem

cells clones but none of satellite myogenic progenitors gave rise to colonies uniformly composed of adipocytes. Shown are representative images of three types of clones derived from clonal satellite cell cultures stained with ORO, and the corresponding percentages from satellite stem cells ($Myf5^{-}$) and satellite myogenic progenitors ($Myf5^{+}$) clones.
See also Figure S1.

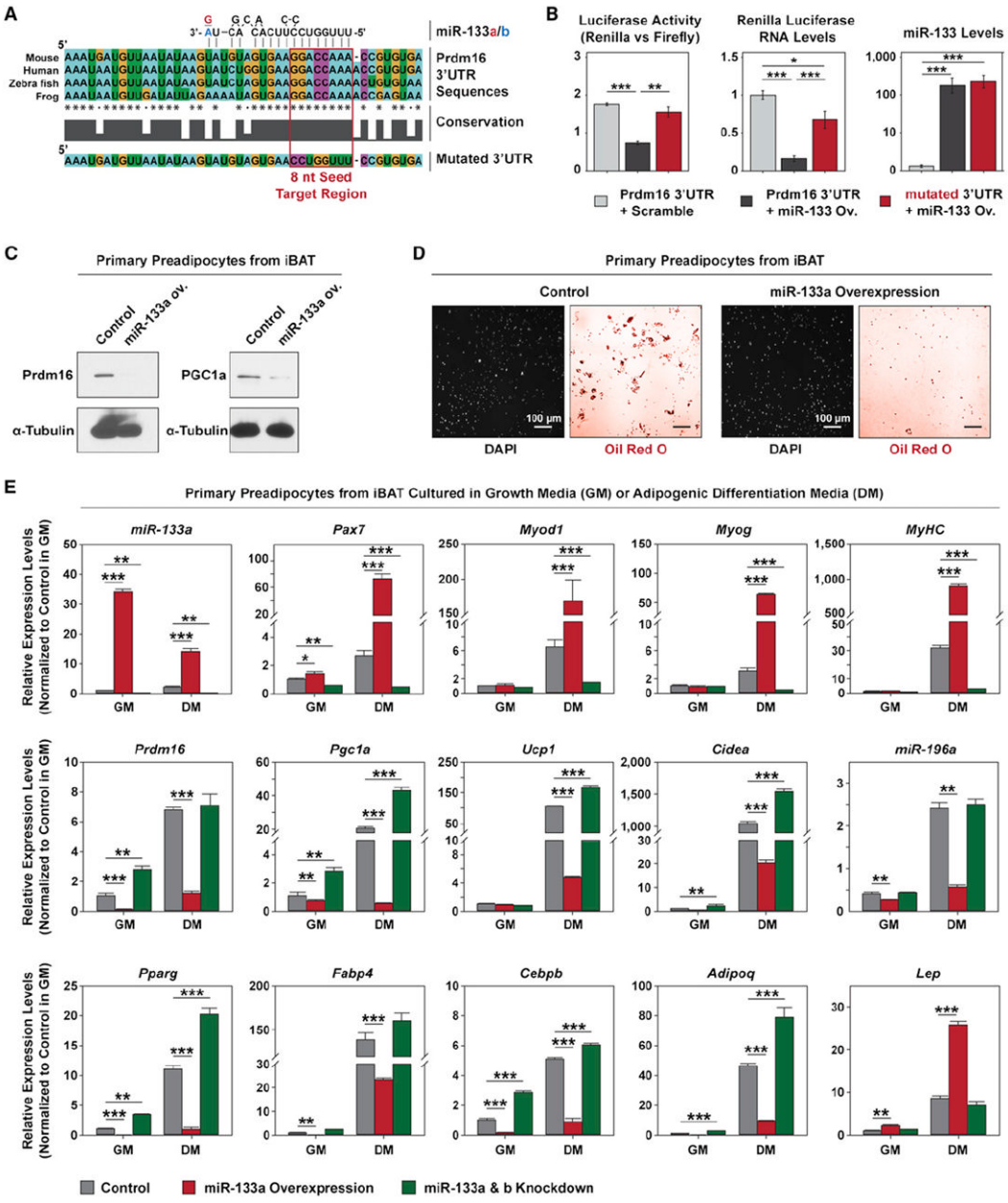

Figure 2. Prdm16 Is Targeted by miR-133

(A) *Prdm16* 3′UTR contains a conserved target site for both miR-133a and miR-133b. The absolutely conserved 8 nt seed sequences in multiple genomes and a mutated seed sequence used in this study (Prdm16_mutUTR) were enclosed in a red frame.

(B) Luciferase assays and RT-qPCR indicate miR-133 targets *Prdm16* 3′UTR and this repression depends on the predicted 8 nt seed sequence. Ectopic miR-133 was overexpressed in HEK293T cells together with *Renilla* luciferase reporter constructs containing either intact or mutated *Prdm16* 3′UTR. The repression of luciferase activity and expression by miR-133 was abolished by mutating the predicted 8 nt seed sequence.

(C) Immunoblots reveals that lentiviral miR-133 overexpression (ov.) in primary brown preadipocytes repressed Prdm16 and Pgc1-α protein levels.

(D) Representative images depict that adipogenic differentiation from primary brown preadipocytes was severely impaired by miR-133 overexpression. ORO staining revealed drastically reduced number of differentiated adipocytes with oil droplets in the miR-133 ov. culture, while DAPI staining of the same fields indicated that same near-confluent density of cells were present for both cultures.
(E) RT-qPCR shows lentiviral overexpression of miR-133 or inhibition of miR-133 by antisense oligos impaired or enhanced brown adipogenic commitment in primary brown preadipocytes, respectively. Notably, impaired brown adipogenic commitment in the miR-133 ov. culture was companied with the emergence of myogenic differentiation, as evidenced by increased expression of myogenic markers (*Pax7, MyoD, Myog, MyHC*), and white adipogenic differentiation, as evidenced by increased expression of *Leptin*.
Error bars, SEM. See also Figure S2.

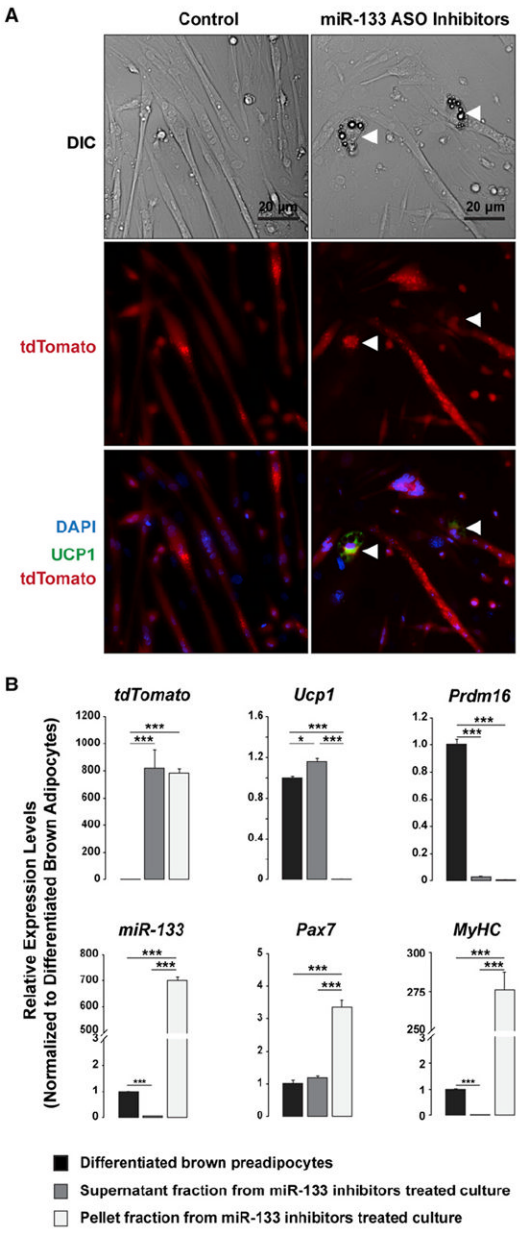

Figure 3. miR-133 Prevents Brown Adipose Determination in Satellite Cells

(A) Inhibition of miR-133 induced satellite cells to differentiate into brown adipocytes (arrowheads) in myofiber cultures under proadipogenic conditions. Myofibers (n > 300) with resident satellite cells were isolated from *Pax7-CreER/R26R-tdTomato* EDL muscles and transfected with mixed inhibitors for miR-133a and miR-133b or a control scramble inhibitor. Lineage-marked satellite cell-derived brown adipocytes (SC_BA) expressed tdTomato and Ucp1.

(B) RT-qPCR reveals gene expression signatures of SC_BAs as compared to those of myotubes and differentiated primary brown adipocytes. miR-133 inhibitor-treated myofiber cultures were centrifuged to separate the supernatant faction enriched for SC_BAs and the pellet fraction which contains mostly myotubes.

Error bars, SEM. See also Figure S3.

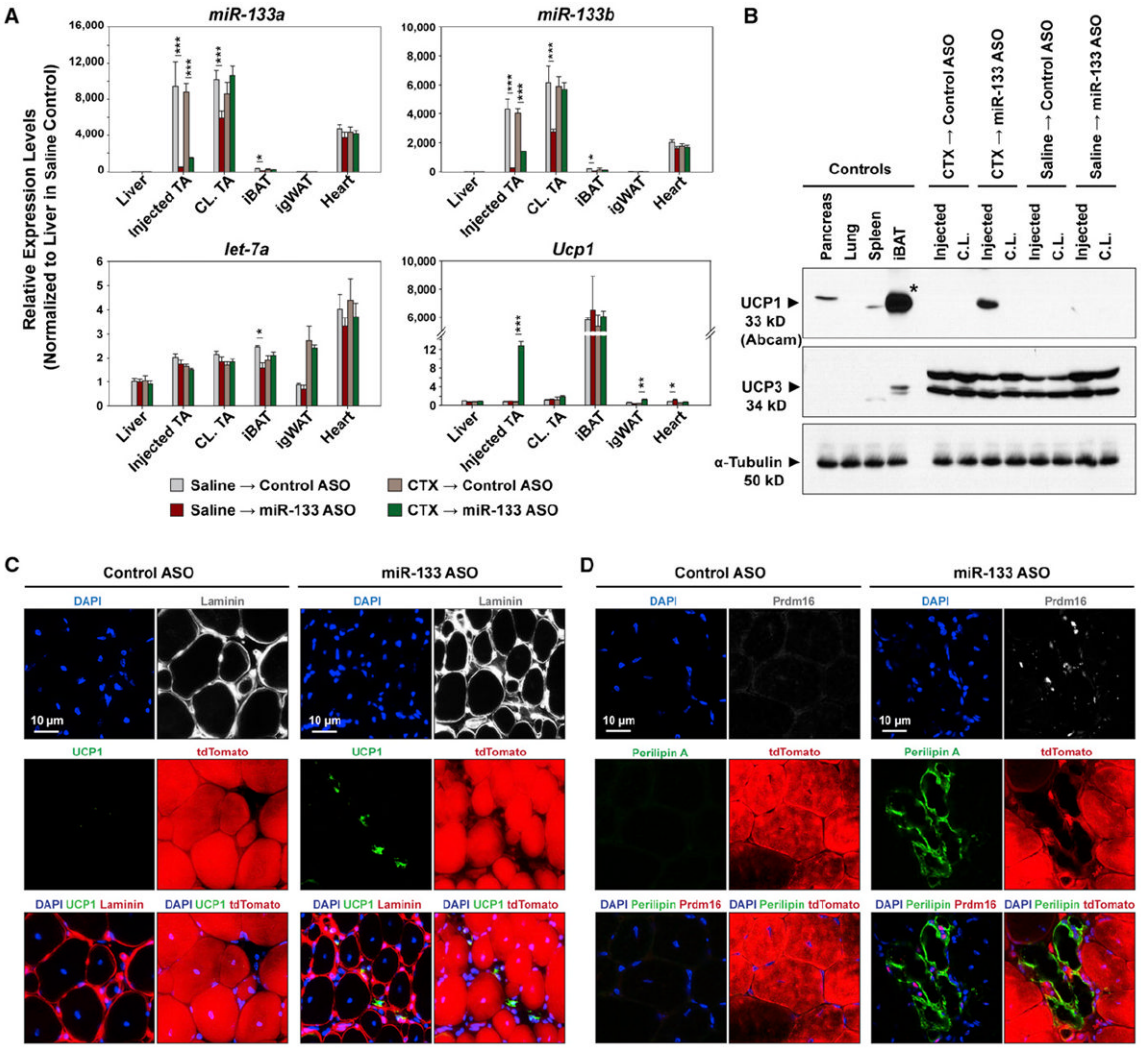

Figure 4. Antagonism of miR-133 Induces Brown Adipose Determination of Satellite Cells during Muscle Regeneration

(A) High efficacy and specificity of miR-133 antagomiR (ASO) in vivo. RT-qPCR indicates reduced expression of both *miR-133a* and *miR-133b*, but not *let-7a* in response to intramuscular miR-133 ASO administration. *Ucp1* mRNA was drastically induced in regenerating TA muscles by miR-133 ASO.

(B) Immunoblots reveal the evident induction of Ucp1, but not Ucp3, in regenerating TA muscles in response to miR-133 ASO treatment. Asterisk denotes that the loading of the iBAT lane on the Ucp1 immunoblot was 1/100 of other lanes to avoid overloading.

(C and D) miR-133 antagonism during muscle regeneration induced satellite cells to differentiate into brown adipocytes located within the muscle interstitium. Representative images of TA muscle cross-sections stained with Ucp1 and Laminin (C) or Prdm16 and Perilipin A (D) together with tdTomato native fluorescence revealed SC_BAs within the muscle interstitium.

Error bars, SEM. See also Figure S4.

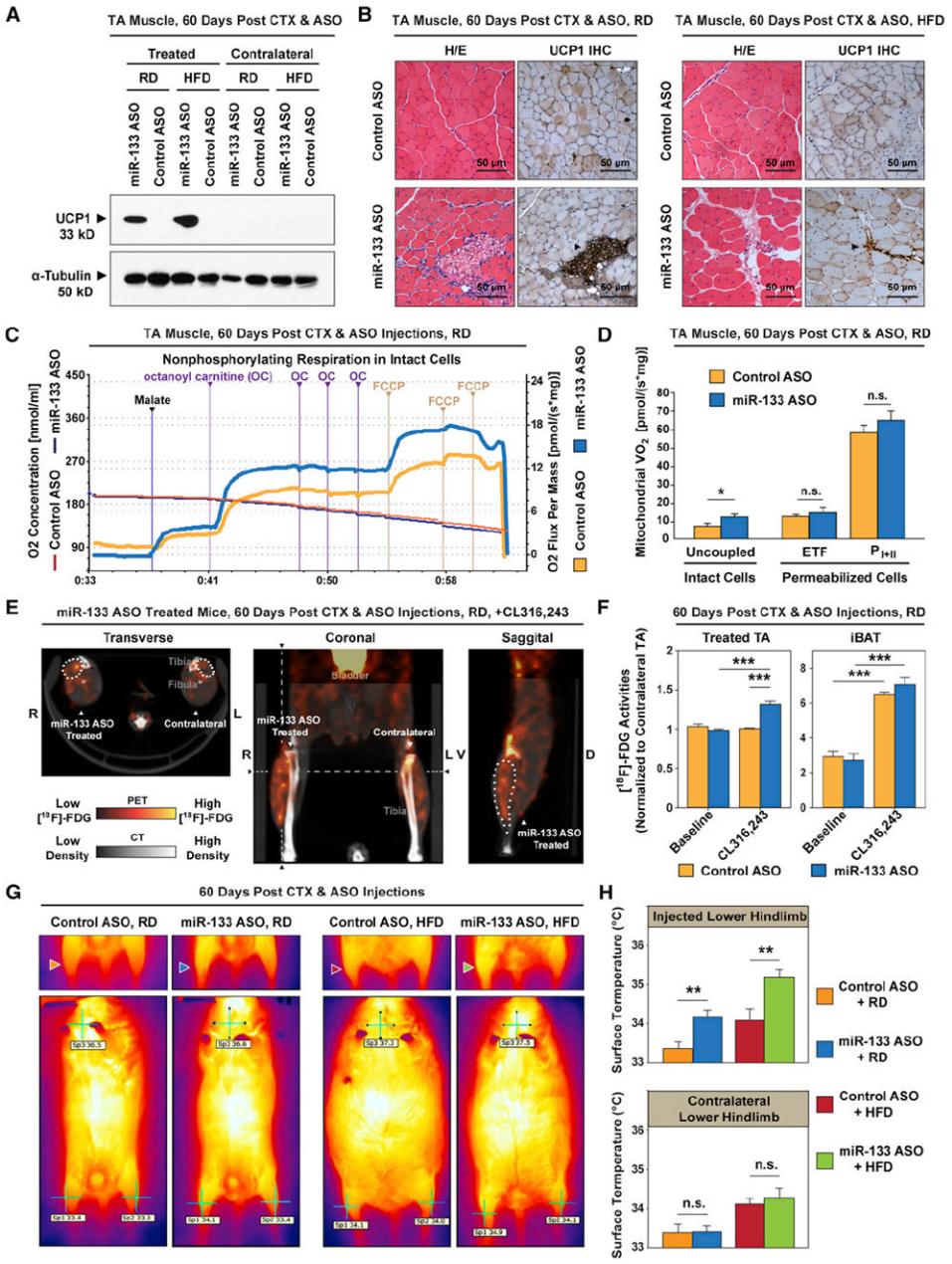

Figure 5. miR-133 Antagonism Induces Metabolically Active Brown Adipocytes in Muscle

(A) Immunoblots reveal the induction of Ucp1 in regenerating TA muscles by miR-133 antagonism in *C57BL/6* mice fed with either a regular diet (RD) or a high-fat diet (HFD). The contralateral TA muscles were included as control.

(B) Hematoxylin and eosin (H/E) staining and immunohistochemistry (IHC) of Ucp1 protein reveal that miR-133 antagonism-induced brown adipocytes located within the muscle interstitium (arrowheads) under both diet conditions.

(C) Representative oxygraph tracings from high-resolution respirometry depict markedly increased uncoupled (nonphosphorylating) respiration in intact (non-permeabilized) miR-133 ASO-treated TA muscles compared to control. Notably, octanoyl carnitine (OC) markedly increased the O_2 consumption in miR-133 ASO-treated TA muscles compared to

control. Responses before reoxygenation (which showed no O_2 diffusion limitation) and titration of antimycin A are shown.

(D) High-resolution respirometry reveals a marked increase of uncoupled respiration in miR-133 ASO-treated TA muscles (intact cells) as well as comparable levels of fatty acid β-oxidation-mediated electron transport through electron-transferring flavoprotein (ETF) and maximal oxidative phosphorylation capacity (P_{I+II}) in control and miR-133 ASO-treated, permeabilized TA muscles (n = 6 per group). Notably, the respiration rate in miR-133 ASO-treated permabilized muscle was comparable to that of control muscle after titration of ADP (ETF).

(E) Representative ^{18}F-FDG microPET/CT images of miR-133 ASO-treated mice depict increased FDG uptake in the ASO-treated TA muscle compared to the contralateral nontreated TA muscle in response to acute CL316,243 treatment. Notably, hot spots with extremely high ^{18}F-FDG activities, presumably representing clusters of active brown adipocytes, were only present within miR-133 ASO-treated TA muscles. Dashed lines denote the levels for transverse and sagittal cross-sections. The position of miR-133 ASO-treated TA muscle was demarcated by dots on these cross-sections.

(F) Quantitative ^{18}F-FDG activities within regions of interest (ROIs) reveal marked increases of FDG uptake in miR-133 ASO-treated TA muscles after acute CL316,243 treatment (n = 5 for miR-133 ASO-treated group, n = 4 for control ASO-treated group). We normalized the ^{18}F-FDG activities within ROIs of treated TA muscles to those of contralateral TA muscles in order to cancel out potential effect of CL316,243 or physical activity on FDG uptake in differentiated muscle cells. ^{18} F-FDG uptake by interscapular BAT (iBAT) was also dramatically induced by CL316,243.

(G) Representative thermographic images depict evident increase of surface temperatures in the miR-133 ASO-treated hindlimbs of mice fed with either a regular diet (RD, blue arrowhead) or a high-fat diet (HFD, green arrowhead) compared to the contralateral hindlimbs or both hindlimbs in control ASO-treated mice. Arrowheads denote ASO treated right hindlimbs. Whole-body thermographic images (lower panels) are shown to denote the representative temperatures at both hindlimbs and neck areas.

(H) Quantitative temperature measurement by thermographic imaging reveals the marked increase of surface temperatures in hindlimbs that received miR-133 ASO treatment (n = 5 per treatment group per diet group).

Error bars, SEM. See also Figure S5.

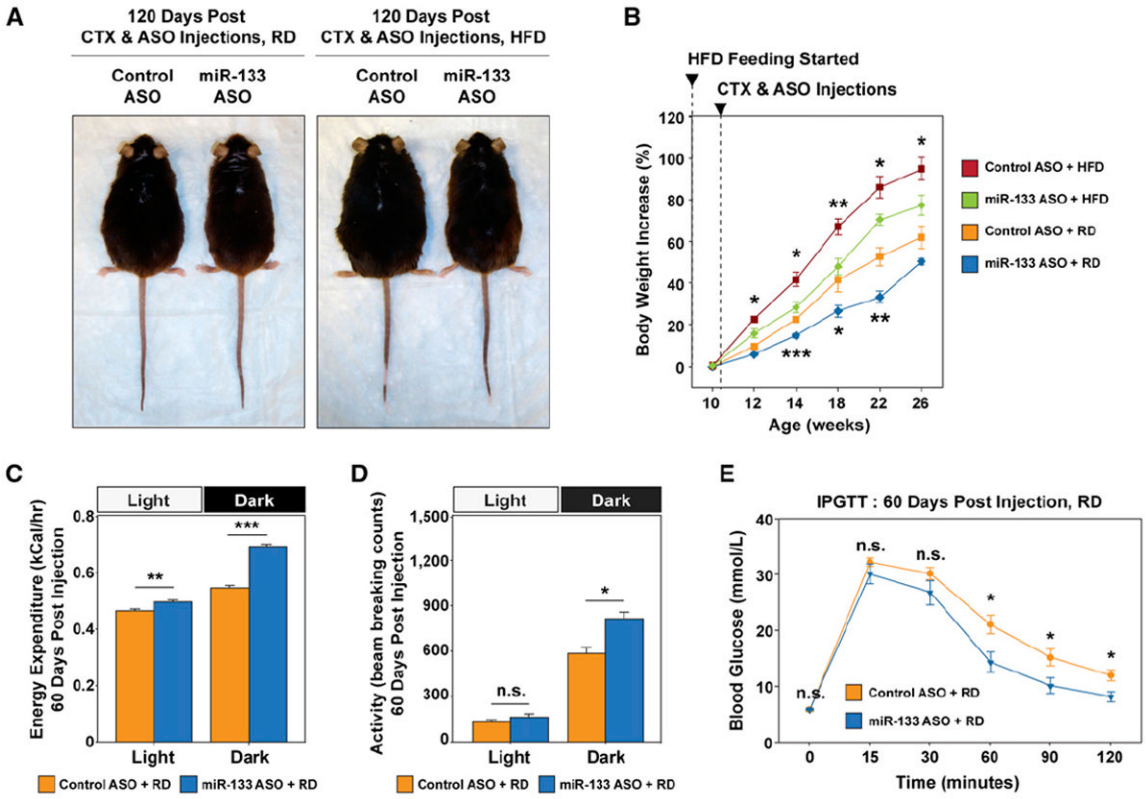

Figure 6. Antagonism of miR-133 during Muscle Regeneration Reduced Adiposity, Increased Total Energy Expenditure, and Improved Glucose Tolerance

(A) Representative images of direct comparisons of *C57BL/6* mice fed the RD or HFD and received control or miR-133 ASO treatment during TA muscle regeneration depict that the miR-133 ASO-treated mice displayed leaner phenotype.

(B) Retarded body weight increase over a 16 week body weight monitoring time course in mice that received miR-133 ASO treatment during TA muscle regeneration (n = 6 per treatment group per diet group).

(C) miR-133 ASO treatment increased total energy expenditure. Indirect calorimetry reveals that mice receiving miR-133 ASO treatment during TA muscle regeneration had a recorded higher energy expenditure than the control mice (n = 5 per group), measured at 22°C during light and dark cycles (fed the RD). Values of total energy expenditure were plotted without normalization to lean body mass.

(D) Physical activities measured within light and dark cycles during indirect calorimetry (C) reveal increased physical activities within the dark cycle for miR-133 ASO-treated mice (fed the RD). Physical activities are presented as arithmetic means of beam-breaking events at X, Y, and Z dimensions.

(E) IPGTT tests for *C57BL/6* mice received either control or miR-133 ASO treatment (fed the RD; n = 6 per group).

Error bars, SEM. See also Figure S6.

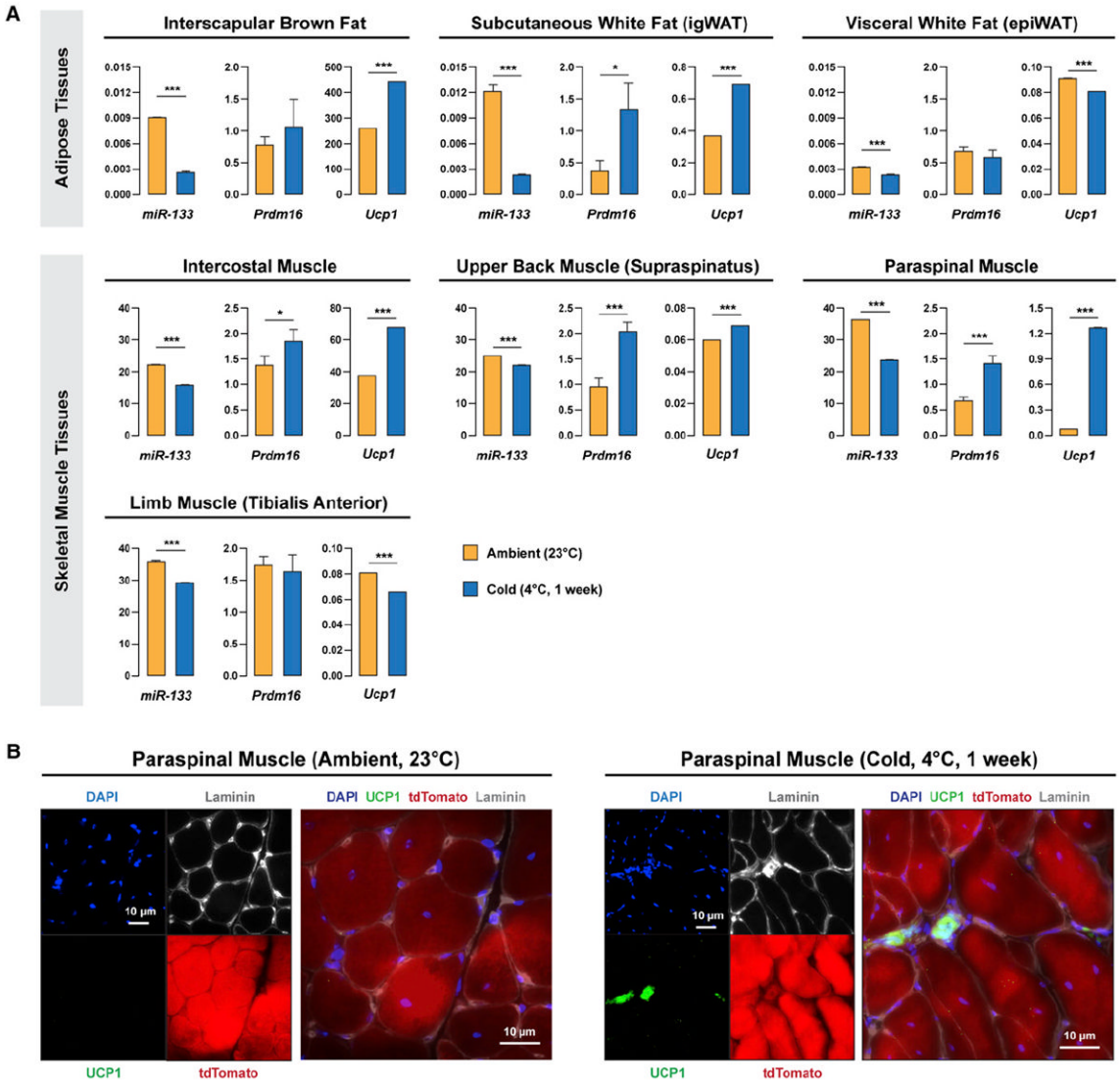

Figure 7. Cold Exposure Downregulates miR-133 Expression in Skeletal Muscles

(A) Cold exposure induced downregulation of *miR-1*33 (*miR-133a* and *miR-133b*) in multiple adipose and muscle tissues and increased expression of brown adipocyte markers, *Prdm16* and *Ucp1*, in subcutaneous WAT and trunk muscles. *C57BL/6* mice were raised under ambient temperature (23°C) or exposed to cold (4°C) for 1 week. Multiple tissues were dissected and investigated by RT-qPCR for the expressions of *miR-133, Prdm16*, and *Ucp1*.

(B) Cold exposure induced satellite cells to differentiate into brown adipocytes located within the muscle interstitium in paraspinal muscles. *Pax7-CreER;R26R-tdTomato* mice were raised under ambient temperature (23°C) or exposed to cold (4°C) for 1 week. Representative images of paraspinal muscle cross-sections stained with DAPI, Ucp1, and Laminin together with tdTomato native fluorescence revealed SC_BAs within the muscle interstitium.

Error bars, SEM.